Turbulent flame–wall interaction: a direct numerical simulation study

A. GRUBER[1]†, R. SANKARAN[2], E. R. HAWKES[3] AND J. H. CHEN[4]

[1]SINTEF Energy Research, 7465 Trondheim, Norway

[2]National Center for Computational Science, Oak Ridge National Laboratory, TN 37831, USA

[3]School of Photovoltaic and Renewable Energy Engineering/School of Mechanical and Manufacturing Engineering, University of New South Wales, Sydney NSW 2052, Australia

[4]Combustion Research Facility, Sandia National Laboratories, Livermore, CA 94550, USA

A turbulent flame–wall interaction (FWI) configuration is studied using three-dimensional direct numerical simulation (DNS) and detailed chemical kinetics. The simulations are used to investigate the effects of the wall turbulent boundary layer (i) on the structure of a hydrogen–air premixed flame, (ii) on its near-wall propagation characteristics and (iii) on the spatial and temporal patterns of the convective wall heat flux. Results show that the local flame thickness and propagation speed vary between the core flow and the boundary layer, resulting in a regime change from flamelet near the channel centreline to a thickened flame at the wall. This finding has strong implications for the modelling of turbulent combustion using Reynolds-averaged Navier–Stokes or large-eddy simulation techniques. Moreover, the DNS results suggest that the near-wall coherent turbulent structures play an important role on the convective wall heat transfer by pushing the hot reactive zone towards the cold solid surface. At the wall, exothermic radical recombination reactions become important, and are responsible for approximately 70 % of the overall heat release rate at the wall. Spectral analysis of the convective wall heat flux provides an unambiguous picture of its spatial and temporal patterns, previously unobserved, that is directly related to the spatial and temporal characteristic scalings of the coherent near-wall turbulent structures.

---

1. Introduction

Flame–wall interaction (FWI) processes are a crucial consideration in the design of modern combustion equipment. Many combustion devices, e.g. gas-turbine combustors or automotive engines, operate in wall-bounded flows and FWI can have strong effects on fuel consumption and pollutant formation which are both central concerns for industry. Flame propagation in the low velocity regions of the boundary layer is indicated as one of the possible causes of flame flashback from the combustion chamber into the mixing zone in gas turbines as discussed in Fritz, Kröner & Sattelmayer (2004). Additionally, spatial and temporal fluctuations of wall temperature induce thermal stresses and strongly affect combustor lifetimes. Finally, typical models of turbulent premixed combustion such as the flame-surface density

† Email address for correspondence: andrea.gruber@sintef.no

approach outlined in Veynante & Vervisch (2002) and Hawkes & Cant (2001) or the G-equation approach discussed in Pitsch (2006) and Peters (1997) do not at present account for the effects of the wall. A better understanding of FWI would directly aid in the design of improved combustion technology as well as the development of predictive combustion models that are required to accelerate the design process.

Yet, the physical mechanisms controlling turbulent FWI and the related wall heat fluxes have not been completely understood because experimental investigations of near-wall turbulent flame structure, flame propagation and flame quenching are very challenging. Obtaining reliable and quantitatively accurate results is very difficult because of problems in performing measurements in the immediate vicinity of the solid surface (the flame quenching distance is typically of the order of hundreds of micrometres). Difficult optical access and spurious scattering from the wall of laser beams results in low signal-to-noise ratio inhibiting accurate measurements in the near-wall region. Moreover, the intrinsic three-dimensionality of the turbulent boundary-layer structures and the resulting interaction with the flame is difficult to capture by two-dimensional optical measurements.

The present work addresses this knowledge gap using direct numerical simulation (DNS) of a turbulent FWI. We study the interaction of a canonical representative FWI configuration to gain fundamental understanding of the processes of FWI, including the effects of wall-turbulence on the structure and propagation speed of the flame, the effects of the flame on the spatial and temporal convective wall heat flux patterns and the influence of detailed chemical kinetic processes at the wall.

The presence of coherent three-dimensional turbulent structures in the wall boundary layer of an inert turbulent flow is well-established knowledge. A comprehensive review on the kinematics of the turbulent boundary layer is given in Robinson (1991). The characteristics of these structures is determined in several seminal studies involving both laboratory experiments (Runstadler, Kline & Reynolds 1963; Kim 1983) and direct numerical simulations (Kim, Moin & Moser 1987; Jiménez & Moin 1991; Kim & Hussain 1994; Orlandi & Jiménez 1994; Jiménez 1998).

As for the interaction between the coherent near-wall turbulent structures and the flame, early experimental measurements in a reactive boundary layer by Ng *et al.* (1982), in spite of the many difficulties mentioned above, suggest the existence of a relationship between the near-wall turbulent structures and flame propagation patterns, although the authors only bring qualitative arguments to support this hypothesis. Laboratory experiments and numerical simulations of FWI for premixed hydrocarbon flames are compared in Ezekoye, Greif & Sawyer (1992), while Enomoto (2002) and Bellenoue *et al.* (2004) address the problem of measuring the typically very small quenching distances with advanced high-definition photography (at a spatial resolution of 20 μm) and derive other quantities, such as the maximum wall heat flux, from adiabatic flame temperature estimates. Because of the difficulties in obtaining accurate near-wall experimental measurements, DNS represents a convenient alternative to experiments in studying the FWI process.

One-dimensional DNS of laminar FWI are reported in Westbrook, Adamczyk & Lavoie (1981), Hocks, Peters & Adomeit (1981), Ezekoye *et al.* (1992), Popp, Smooke & Baum (1996) and Popp & Baum (1997). The focus of these studies is on premixed laminar hydrocarbon flames propagating perpendicular to the wall and stagnating on it: this configuration is also known as head-on quenching (HOQ). These studies concur that radical recombination at the wall, characterized by low activation energy reactions, plays an important role in the FWI process and that a single-step chemistry approach, lacking detailed information about radical recombination reactions, fails to

predict FWIs correctly. Quenching of premixed and non-premixed $H_2 + O_2$ laminar flames onto an inert wall is simulated using detailed chemical kinetics by Dabireau *et al.* (2003), and again, the importance of radical recombination reactions at the wall is emphasized. For the $H_2 + O_2$ flame they found similar qualitative quenching behaviour as observed earlier in hydrocarbon–air flames but quantitatively different non-dimensional quenching parameters (the quenching Péclet number P_Q and the non-dimensional quenching wall heat flux F_Q).

Multi-dimensional DNS of turbulent FWI are very expensive computationally, and therefore, only few such investigations are reported in the literature. Moreover, because of their high cost (and in spite of the conclusions reached in the one-dimensional studies mentioned above), all reported multi-dimensional DNS of turbulent FWI have been restricted to simple one-step chemical kinetics and small physical domains (limited to the 'minimal' channel dimensions defined in Jiménez & Moin 1991). For example, Poinsot, Haworth & Bruneaux (1993) reported a two-dimensional DNS of HOQ in a pseudo-turbulent reactive boundary layer while Bruneaux *et al.* (1996) studied three-dimensional HOQ of a back-to-back premixed flame propagating in constant density turbulent channel flow. Alshaalan & Rutland (1998, 2002) investigated sidewall quenching (SWQ) of a three-dimensional v-shaped premixed flame anchored in weakly turbulent Couette flow. These numerical experiments have provided a wealth of information, but detailed kinetics simulations are still needed to account for the important effects of radical recombination reactions.

In the present study DNS is used to study the evolution of a three-dimensional, v-shaped, premixed H_2–air flame that is anchored in a low-Reynolds-number turbulent Poiseuille flow and its interaction with an isothermal wall. The simulated turbulent reactive flow is characterized by variable thermo-physical properties and described by a detailed hydrogen–air chemical kinetics mechanism. The focus of the study is on improving the understanding of the flame propagation characteristics and structure as a function of the distance from the wall. Moreover, the convective wall heat flux spatial and temporal patterns induced by FWI are analysed both in physical and spectral space. Accordingly, this study builds on the previous knowledge and provides a better understanding of the FWI process in two respects. First, a detailed chemical kinetics approach is adopted. Given the clear indications from previous studies concerning one-dimensional laminar FWIs, modelling of the combustion process with detailed chemical kinetics is adopted in this work since it is necessary for a proper representation of radical species diffusion and recombination at the wall. For example, key parameters such as the maximum wall heat flux and flame quenching distance are not correctly predicted by the single-step chemistry approximation (used in Bruneaux *et al.* 1996; Alshaalan & Rutland 1998). Second, sidewall quenching is simulated: the back-to-back flame HOQ configuration used by Bruneaux *et al.* (1996) does not allow statistically stationary analysis of the FWI. Relevant quantities have to be averaged from several different realizations of the initial turbulence to ensure their independence from the initial conditions. The v-shaped flame configuration adopted in the present work is immersed in a fully developed turbulent-plane channel flow characterized by considerably larger dimensions than the minimal channel of Jiménez & Moin (1991). This enables statistically stationary results averaged both in time and in the spanwise homogeneous direction, and statistical analysis of the spatial and temporal correlation between the near-wall vortical streaky structures and the flame brush.

This remainder of the paper is organized as follows: the governing equations and the problem formulation are presented in §2. The numerical methods in the DNS

n	Reaction	B	a	E_a
1	$O_2 + H \Leftrightarrow OH + O$	3.547×10^{15}	-0.406	1.6599×10^4
2	$H_2 + O \Leftrightarrow OH + H$	0.508×10^5	2.67	0.629×10^4
3	$OH + H_2 \Leftrightarrow H + H_2O$	0.216×10^9	1.51	0.343×10^4
4	$H_2O + O \Leftrightarrow 2OH$	2.97×10^6	2.02	1.34×10^4
5	$H_2 + M \Leftrightarrow 2H + M$	4.577×10^{19}	-1.40	1.0438×10^5
6	$2O + M \Leftrightarrow O_2 + M$	6.165×10^{15}	-0.50	0.0
7	$H + O + M \Leftrightarrow OH + M$	4.714×10^{18}	-1.00	0.0
8	$OH + H + M \Leftrightarrow H_2O + M$	3.800×10^{22}	-2.00	0.0
9	$O_2 + H(+M) \Leftrightarrow HO_2(+M)$	1.475×10^{12}	0.60	0.0
10	$H + HO_2 \Leftrightarrow O_2 + H_2$	1.66×10^{13}	0.00	0.823×10^3
11	$H + HO_2 \Leftrightarrow 2OH$	7.079×10^{13}	0.00	2.95×10^2
12	$O + HO_2 \Leftrightarrow OH + O_2$	0.325×10^{14}	0.00	0.0
13	$OH + HO_2 \Leftrightarrow O_2 + H_2O$	2.890×10^{13}	0.00	-4.970×10^2
14	$2HO_2 \Leftrightarrow O_2 + H_2O_2$	4.200×10^{14}	0.00	1.1982×10^4
15	$H_2O_2(+M) \Leftrightarrow 2OH(+M)$	2.951×10^{14}	0.00	4.843×10^4
16	$H + H_2O_2 \Leftrightarrow OH + H_2O$	0.241×10^{14}	0.00	0.397×10^4
17	$H + H_2O_2 \Leftrightarrow H_2 + HO_2$	0.482×10^{14}	0.00	0.795×10^4
18	$O + H_2O_2 \Leftrightarrow HO_2 + OH$	9.550×10^6	2.00	3.970×10^3
19	$OH + H_2O_2 \Leftrightarrow H_2O + HO_2$	5.800×10^{14}	0.00	9.557×10^3

TABLE 1. The complete nine species, 19 reactions hydrogen–air chemical kinetics mechanism from Li *et al.* (2004).

code, S3D, used to perform the present simulations are briefly discussed in §3. Results from DNS are presented in §4. Finally, conclusions and recommendations for further work are presented in §5.

2. Mathematical description and configuration

The Navier–Stokes equations in their compressible formulation are solved in a three-dimensional computational domain to simulate SWQ of a v-shaped 'turbulent' premixed H_2–air flame anchored in fully developed plane channel turbulence and, for comparison, the same set of equations is solved on a one-dimensional computational domain to simulate HOQ of a plane 'laminar' premixed H_2–air flame. The homogeneous chemical reactions in the gaseous phase are described by a detailed chemical kinetics mechanism for hydrogen combustion in air by Li *et al.* (2004) that is reported in table 1. The mechanism contains nine species and 19 elementary reaction steps (see table 1 for details). Note that nitrogen is assumed inert in this context (NO_x-formation reactions are not included). The scheme incorporates gas-phase low-temperature (zero activation energy) radical recombination reactions. Heterogeneous surface chemistry and the third body effect of the wall are deliberately neglected so as to provide a sharp focus for the investigation as a limiting case of an inert surface. It is recognized that this represents an approximation, but consideration of surface chemistry would introduce the influence of the surface material details as an additional parameter and limit the generality of the findings considering that any number of materials might be applied in practical combustors.

Thermodynamic properties are modelled as polynomial functions of temperature and transport coefficients as described in the CHEMKIN and TRANSPORT packages respectively (see Kee *et al.* 1999). No attempt is made to incorporate the effects of radiative heat transfer into this discussion.

Three-dimensional turbulent FWI	$Re_\tau = 180$	$L_x \times L_y \times L_z = 7H \times 2H \times 3H$	$N_x \times N_y \times N_z = 600 \times 200 \times 280$
	$T_w = T_u = 750$ (K)	$\phi = 1.5$	$Da = 0.26$
	$S_l/U_c = 0.15$	$u_\tau/S_l = 0.355$	$u_\tau/U_c = 0.053$
	$\delta_l/H = 0.069$	$x_{anc}^+ = 180$	$y_{anc}^+ = 180$

TABLE 2. DNS parameters for the three-dimensional case: H is the channel half-width, subscript 'anc' indicates the spatial coordinates of the flame anchor.

The approaching flow Reynolds number is $Re_0 \sim 3200$, based on the centreline velocity U_c and the channel half-width H. This corresponds to a friction Reynolds number $Re_\tau \sim H/\delta_\nu \sim 180$ (where δ_ν is the viscous length scale). All turbulent quantities used below for non-dimensionalization characterize the turbulent flow of the fresh reactants upstream of the flame. The Damköhler number (ratio of a chemical to dynamical time scale) that characterizes the turbulent flame in the boundary layer is $Da \sim 0.26$. This Damköhler number is based on the freely propagating laminar flame time scale ($t_l = \delta_l/S_l \sim 1.67\mathrm{e}^{-05}$ (s)) and on the wall time scale uniquely defined from the turbulent channel flow of the fresh reactants ($t_w = \nu/u_\tau^2 \sim 4.33\mathrm{e}^{-06}$ (s)). In these expressions ν is the kinematic viscosity of the reactants, u_τ is its friction velocity, δ_l and S_l are the laminar flame thickness and velocity, respectively. The present choice of the wall time scale in the definition of the Damköhler number is uniquely defined for any specific turbulent channel flow configuration. Alternative definitions based on the values of the integral t_T and Kolmogorov t_K time scales, commonly used in homogeneous isotropic turbulence to determine the Damköhler and Karlovitz numbers ($Da(t_T/t_l), Ka(t_l/t_K) = 1/Da(t_K/t_l)$), vary between the channel wall and the centreline and, therefore, do not provide a unique ratio between the chemical and dynamical time scales for a specific FWI configuration. The turbulence and flame parameters studied here are similar to the simple-chemistry flame that is simulated in Alshaalan & Rutland (2002) for a Couette flow configuration. Other relevant parameters of the direct simulation are listed in table 2. Note that the non-dimensional centreline velocity is $u_c^+ \sim U_c/u_\tau \sim 19$.

The premixed H_2–air mixture in the approaching flow is characterized by an equivalence ratio, ϕ, equal to 1.5. The temperature of the wall and of the cold stream of reactants is pre-heated to 750 K. The choices for ϕ and the temperature have been made to result in a high flame-speed, allowing a high approach flow velocity, short channel transit-time and, ultimately, lower computational cost. Moreover, 750 K is the nominal temperature of the combustion air delivered by the compression stage in large, stationary gas turbines for power generation in the 200–400 MW range.

The turbulent hydrogen–air mixture enters the channel from a non-reflecting inflow boundary. An auxiliary DNS of inert fully developed turbulent-plane channel flow (driven by an effective streamwise pressure gradient) is used both to validate the present code against previous results by Kim *et al.* (1987) and to provide the reactive cases with an initial turbulence field and inlet turbulence. Results from this auxiliary simulation are shown in figure 1. The normalized mean velocity profile is plotted against the channel width in figure 1(*a*), the same quantity is presented using a log scale for the channel half-width in figure 1(*b*). The normalized Reynolds stress term and the temperature fluctuation normalized by the wall temperature are shown in figures 1(*c*) and 1(*d*), respectively. Figure 1(*d*) indicates that the peak in the temperature fluctuation for the boundary-layer fluid equals 0.1 % of the wall temperature. The agreement is very good, demonstrating that adequate resolution has
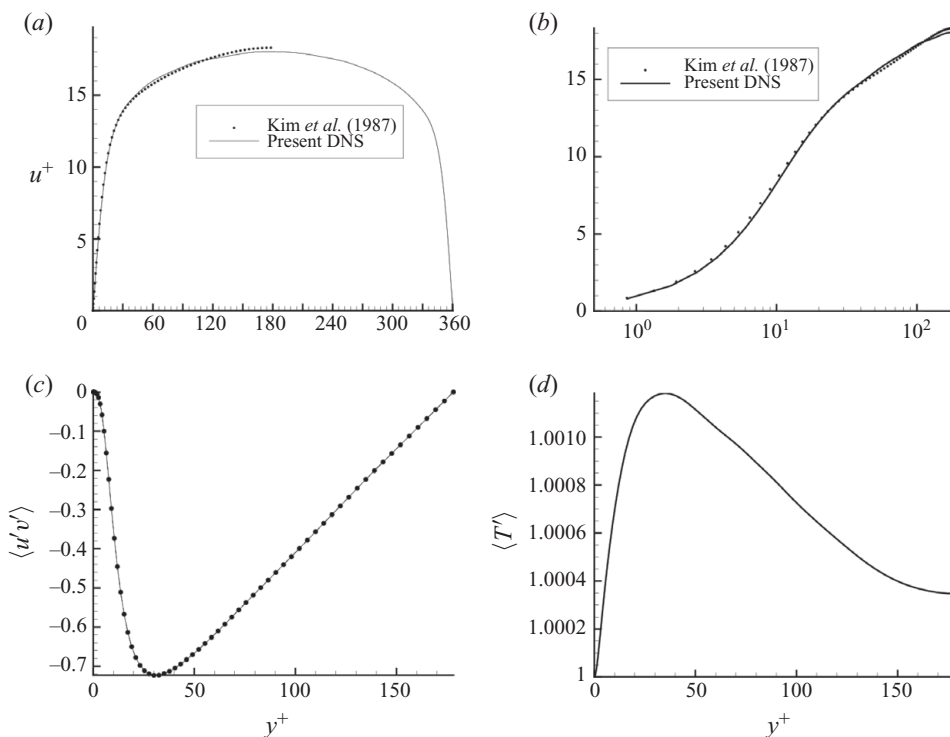
FIGURE 1. Comparison of normalized mean velocity profiles (*a*, *b*) and Reynolds stress (*c*) between the auxiliary inert turbulent channel flow simulation of the present study and the database from Kim *et al.* (1987). Additionally, for the same inert turbulent channel flow, the fluid temperature fluctuation level is shown normalized by the wall temperature (*d*).

been employed in this study. Further details about the inert channel flow case can be found in Gruber (2006).

The velocity fluctuations imposed at the channel inlet are obtained by temporal sampling of the 'temporally evolving turbulence' at a fixed streamwise location in the auxiliary inert simulation. This approach, which permits eddies to 'evolve' on the boundary, provides a more realistic description of the incoming turbulence compared with the usual practice of convecting a turbulence field at one time instant into the domain by Taylor's hypothesis.

Navier–Stokes characteristic boundary conditions (NSCBC) are implemented based on Poinsot & Lele (1992) and Sutherland & Kennedy (2003). The boundary conditions are non-reflecting at the inflow ($x = 0$) and outflow ($x = L_x$) planes, no-slip isothermal solid surface at the wall boundaries ($y = 0$ and $y = L_y$) and periodic in the spanwise direction ($z = 0$ and $z = L_z$). The wall is assumed to be impermeable, so the wall-normal mass flux of all chemical species is set to zero.

The reactive case is initialized by setting pressure to 1 atm everywhere and by imposing an instantaneous velocity fluctuation field computed in the inert simulation. Density, temperature and composition fields are initialized in the shape of a v-flame propagating downstream of a flame anchor. A progress variable function c is used in the initialization to map all points in the three-dimensional domain to a one-dimensional CHEMKIN PREMIX (Kee *et al.* 1999) solution of the H_2–air flame under investigation. The adopted initialization technique yields marginally

incorrect initial fields and a 'settling' time interval of one channel transit time $(t_c = L_x/U_c)$ is required before sampling of the solution commences. Results are sampled every 1.8 wall time units, t_w, as suggested in Alshaalan & Rutland (2002) for a similar configuration. The sampling interval equals two channel transit times, $2t_c = 14H/U_c \sim 1.0e^{-03}$ (s). The numerical integration time step is fixed to a value, $\Delta t = 4.0e^{-09}$ (s) in the reactive case, and to $\Delta t = 1.0e^{-08}$ (s) in the inert auxiliary simulation, corresponding to 1082 and 433 time steps every wall time unit, t_w, respectively.

The three-dimensional Cartesian grid is uniform in the streamwise and spanwise directions and is refined in the wall-normal direction near the opposite solid surfaces using a 'tanh' mapping. The first point off the wall is at $y^+ = 0.5$ where the superscript $+$ indicates non-dimensionalization by the viscous length scale. There are two points within $y^+ = 1$ and 13 points within $y^+ = 10$ to satisfy the resolution requirements in the viscous layer (Moser, Kim & Mansour 1999). The grid resolution is $\Delta x^+ = 2.0$ (31 μm), $\Delta y^+ = 0.4$–3.5 (6–56 μm) and $\Delta z^+ = 2.0$ (31 μm). The grid is only mildly stretched by a factor of 9 in the wall normal direction. Relatively 'light' stretching (a factor of 100 is usual in other contexts) is used to accurately represent the flame which requires high spatial resolution throughout the channel, including near the centreline.

In the present DNS a flame 'anchor' is required because, for the target Reynolds number and chosen channel dimension, the mean streamwise flow velocity at the channel centreline is considerably larger than the turbulent premixed flame propagation speed. The flame anchor is obtained by smoothly imposing the adiabatic flame temperature and burned composition in a cylindrical region of the domain characterized by a diameter of 0.25 mm (approximately 16 wall units). The anchor is placed at the channel centreline (equidistant from the walls), at 180 wall units downstream of the channel inlet, and it extends throughout the entire spanwise direction. Since the focus of the present study relates primarily to the FWIs rather than to the flame behaviour in the vicinity of the anchor point, the specifics of the flame anchor are such that they do not significantly affect the downstream FWI results. A similar flame anchor was used in a prior computational study of an unconfined v-flame by Domingo *et al.* (2005).

3. The direct numerical simulation code

The parallel DNS code, S3D, developed at the Combustion Research Facility at Sandia National Laboratories (Chen *et al.* 2009) is used to perform the present simulations. The code has been used for a range of studies including premixed flames (Echekki & Chen 1999; Hawkes & Chen 2004, 2005), non-premixed flames (Lignell *et al.* 2007; Hawkes *et al.* 2006) and autoignition (Echekki & Chen 2003; Sankaran *et al.* 2004).

The code S3D is written in FORTRAN 90 and uses the Message Passing Interface (MPI) for inter-process communication in parallel execution. The algorithm implemented in S3D solves the Navier–Stokes equations for a compressible fluid in conservative form on a structured Cartesian mesh in one, two or three spatial directions. Spatial derivatives are computed with an eighth-order explicit centred finite difference scheme (third-order one-sided stencils are used at the domain boundaries in the non-homogeneous directions) in conjunction with a tenth-order explicit spatial filter, as described in Kennedy & Carpenter (1994), to remove high frequency noise and reduce aliasing error. A fourth-order six-stage explicit Runge–Kutta scheme, described in Kennedy, Carpenter & Lewis (2000), is used for time integration.

4. Results

In the present section results from DNS of laminar and turbulent FWI configurations are presented. The laminar FWI case is first reported here as a reference case and compared against previous studies by other research groups on the same topic. Subsequently the turbulent FWI results are presented, which constitutes the primary focus of this study.

The instantaneous convective wall heat flux Φ_w is defined as

$$\Phi_w = -\lambda \left(\frac{\partial T}{\partial y} \right)_w, \qquad (4.1)$$

where y is the wall-normal direction, T is the gas mixture temperature and λ is the local thermal conductivity of the gaseous mixture. The 'mean' convective heat flux into the solid surface of a combustion chamber is mainly attributed to the hot products of combustion along the combustor walls downstream of the flame. By contrast, the 'maximum' convective wall heat fluxes, which are more difficult to capture experimentally and by conventional modelling, are due to the FWI process in the region where the flame impinges onto the wall. The FWI is an intrinsically transient process in which the hot flame brush propagates towards the cold wall and quenches in its vicinity, at a quenching distance y_Q. This occurs locally where exothermic zero-activation-energy radical recombination reactions result in a shortage of radicals, accompanied by a tenfold increase in the heat release rate. The presence of the wall acts as a heat sink, and hence the large amount of thermal energy released in the reacting mixture by the radical recombination reactions rapidly conducts into the solid surface causing a peak in the heat transfer to the wall, the quenching wall heat flux $\Phi_{w,Q}$. The FWI process can be conveniently described by two quenching parameters – the quenching Péclet number, $Pe_Q = y_Q/\delta_Q$, and the quenching wall heat flux, $F_Q = \Phi_{w,Q}/P_Q$. Note that in the present study the quenching distance and quenching wall heat flux are non-dimensionalized by the flame thickness at the quenching limit, δ_Q, and by the flame power, $P_Q = \rho_u S_l c_{p,mix}(T_b - T_u)$.

4.1. *Laminar flame–wall interaction*

A laminar FWI is first simulated in a one-dimensional DNS with detailed hydrogen-air chemistry to provide a reference for the three-dimensional turbulent FWI DNS. In this configuration a planar laminar flame propagates towards the wall at a normal angle with the solid surface (HOQ configuration). The temperature and mixture conditions are the same as in the three-dimensional DNS. An open non-reflecting boundary is placed on the boundary ($x = 2$ mm). The one-dimensional uniform grid consists of 300 points providing a spatial resolution of approximately 7 μm that is sufficient to resolve the flame structure with more than ten grid points. CHEMKIN PREMIX solutions for a freely propagating H_2-air flame are used to initialize the one-dimensional DNS.

Figure 2 shows temperature profiles (*a*) and overall heat release rate (*b*) for different times, illustrating the time-dependence of a nominal quenching process. Initially the flame propagates freely in the undisturbed fluid away from the wall. However, when the flame–wall distance becomes smaller than ten times the flame thickness the flame is affected by the presence of the wall, decelerating and becoming increasingly thinner until quenching occurs at a flame–wall distance of approximately two flame thicknesses (for the present hydrogen flame). The quenching process involves a tenfold increase in the overall flame heat release rate as zero-activation-energy, exothermic, radical recombination reactions occur at the 'cold' wall surfaces and deplete the reaction
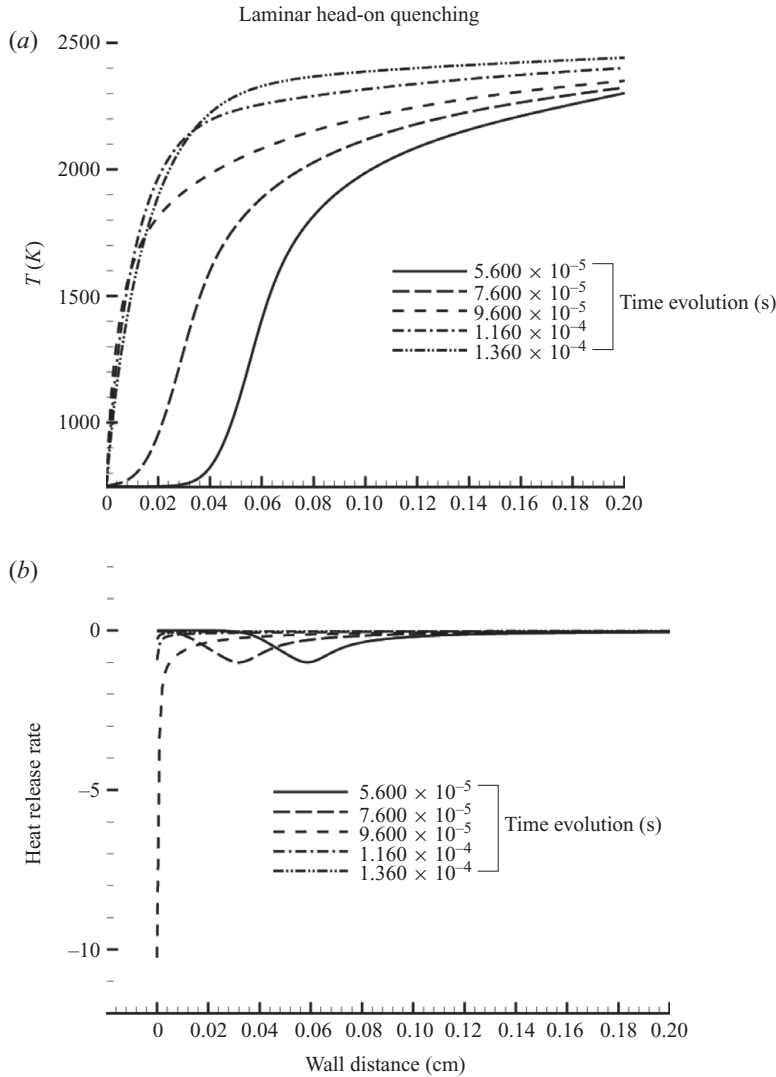
FIGURE 2. Case LW6: time evolution of temperature (*a*) and normalized heat release rate (*b*). The heat release rate of the freely propagating flame is used for normalization. Quenching of the laminar flame takes place at time $t = 9.6e^{-5}$ (s).

zone of the necessary radical species. The profiles of reactionwise heat release rates shown in figure 3(*a*) for reactions 8, 9 and 11 and in figure 3(*b*) for all remaining reactions illustrate quantitatively that radical recombination reactions are responsible for about 70 % of the tenfold increase in overall heat release rate at quenching. These one-dimensional results are similar to previous studies and more detailed discussion on this topic is given in Dabireau *et al.* (2003). We find that the quenching parameters are $Pe_Q = 1.4$ and $F_Q = 0.12$. The parameters are similar to the values $Pe_Q = 1.7$ and $F_Q = 0.129$ reported in Dabireau *et al.* (2003) for $H_2 + O_2$ flames. Consistent with Dabireau *et al.* (2003), the quenching parameters demonstrate that hydrogen is a fuel with characteristics very different from those of other common hydrocarbon fuels, e.g. typically $Pe_Q \sim 3.0$ and $F_Q \sim 0.3$ for methane flames.
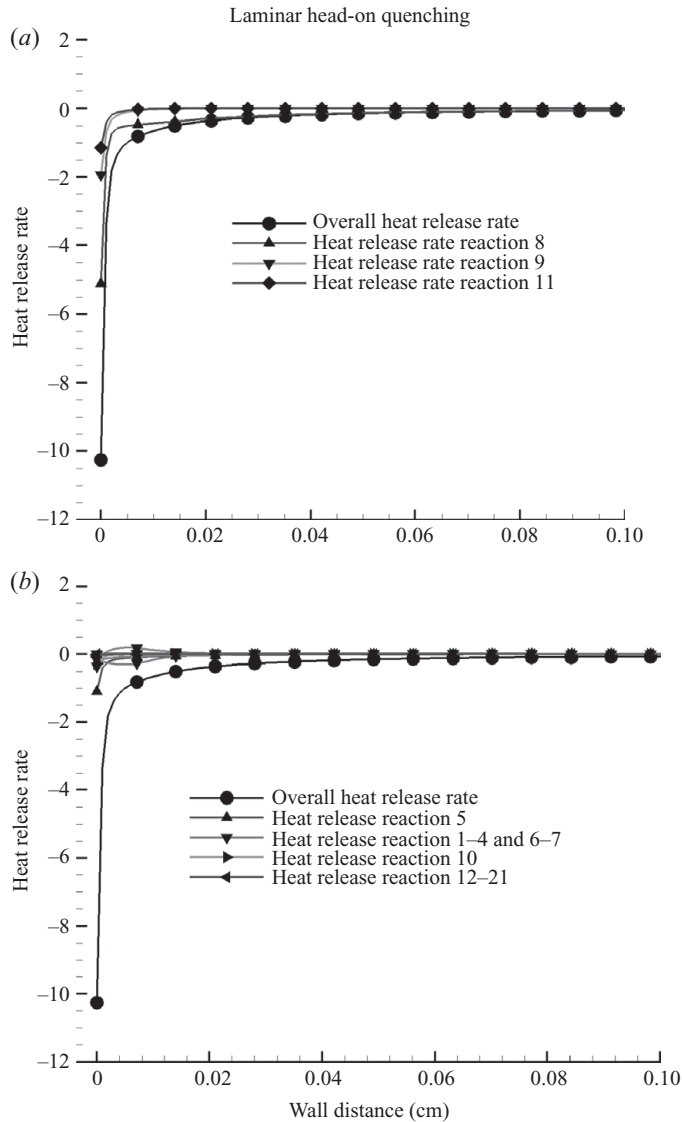
FIGURE 3. Case LW6: normalized overall heat release rate and heat release rate for the radical recombination reactions 8, 9 and 11 (*a*). Normalized overall heat release rate and heat release rate for reactions 1–7, 10 and 12–21 (*b*). The heat release rate of the freely propagating flame is used for normalization.

4.2. *Turbulent flame–wall interaction*

The three-dimensional DNS of the turbulent FWI configuration is represented in figure 4, and in the following, the x, y and z directions denote streamwise, wall-normal and spanwise directions, respectively. The results are analysed both by visual inspection of the instantaneous fields of relevant kinematic and scalar quantities, providing a qualitative understanding of non-local interactions between the boundary-layer coherent wall structures and the flame, and by a more rigorous statistical analysis of the data providing a quantitative description of the physical processes. These approaches are applied in the following sections to determine the characteristics
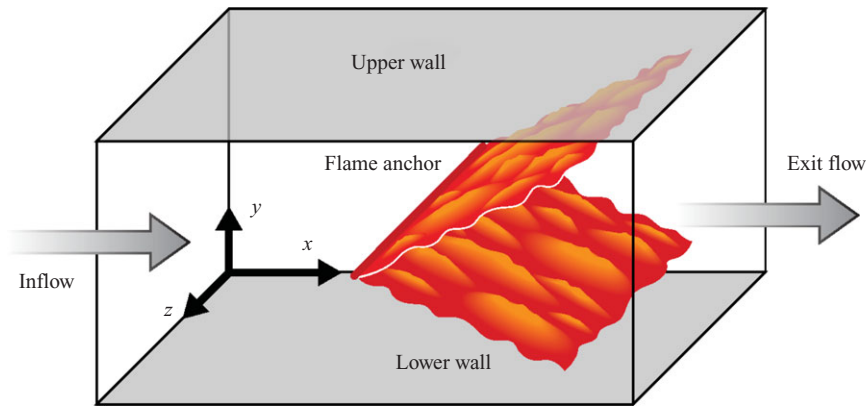
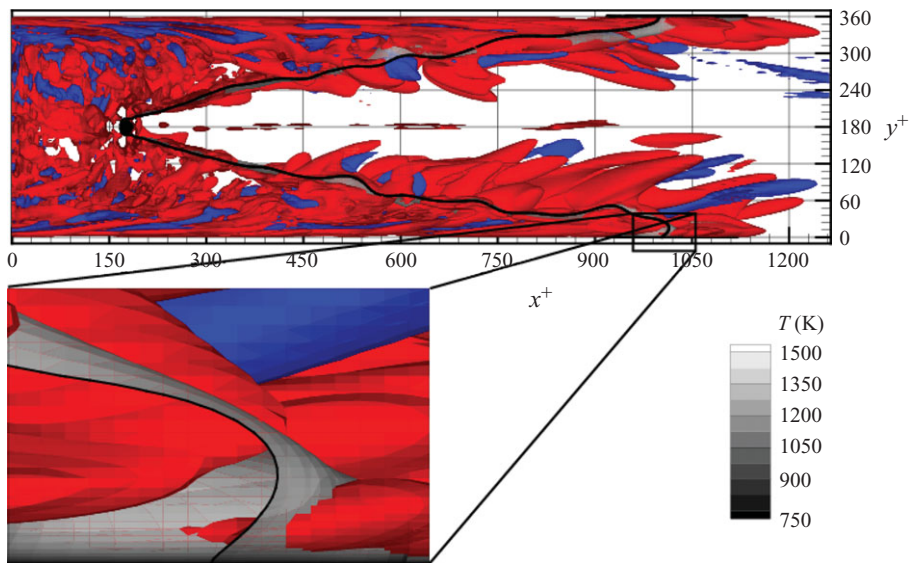FIGURE 4. Pictorial representation of the plane channel with the
flame anchor.

FIGURE 5. Instantaneous snapshot of the computational domain, the flow direction is from left to right: blue and red isosurfaces represent vortical structures represented by the second invariant of the velocity gradient tensor. The v-shaped isosurface represents the locus of the reaction progress variable at $C = 0.7$ demarcating the instantaneous flame shape and position. The grey-scale colour levels indicate the local temperature.

of flame propagation in the turbulent boundary layer and to analyse the convective heat fluxes into the solid wall.

4.2.1. *Flame structure, thickness and propagation*

Figure 5 is an instantaneous snapshot showing representative boundary-layer structure and their spatial orientation relative to the flame in the computational domain: the flow is from left to right. The blue and red isosurfaces represent vortical structures of the flow, characterized by opposite signs of rotation and rendered by the second invariant of the velocity gradient tensor Hunt, Wray & Moin (1988)
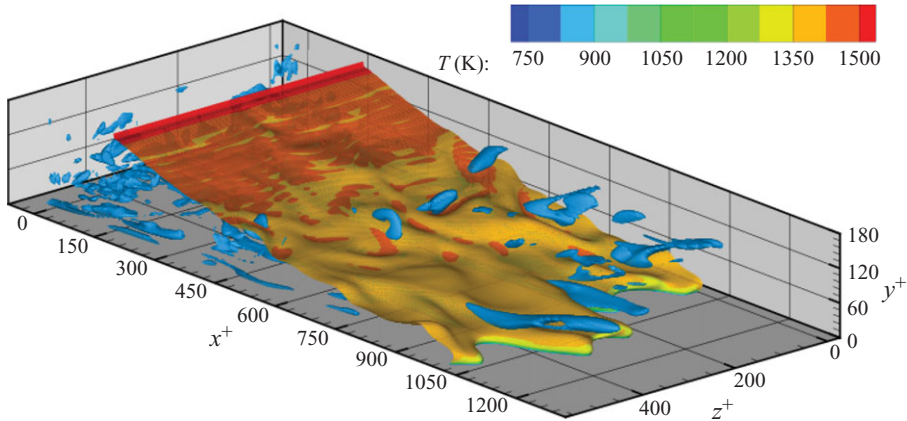
FIGURE 6. Instantaneous snapshot of the lower half of the computational domain, the flow direction is from top left to bottom right: light blue isosurfaces represent vortical structures represented by the second invariant of the velocity gradient tensor. The flame surface is demarcated by the reaction progress variable at $C = 0.7$ and is coloured by the local temperature.

defined as

$$Q = \tfrac{1}{2} \left(A_{ii}^2 - S_{ij} S_{ij} - W_{ij} W_{ij} \right), \tag{4.2}$$

where A_{ij} is the velocity gradient tensor, $S_{ij} = (A_{ij} + A_{ji})/2$ is the rate of strain tensor and $W_{ij} = (A_{ij} - A_{ji})/2$ is the rate of rotation tensor.

The v-shaped isosurface is the reaction progress variable evaluated at $C = 0.7$ and demarcates the flame. In premixed flames, the reaction progress variable C is typically defined based on temperature or species mass fraction, and is equal to zero in the fresh reactants and increases monotonically to unity in the fully burned products. The present choice of the reaction progress variable C is based on the concentration of the fuel, H_2. This choice was made amongst the other possible choices of H_2O and O_2 because in the present conditions, the hydrogen mass fraction was found to best track the location of maximum heat release rate. The effect of the flame on the approaching turbulence is clearly visible in figure 5, causing a marked increase in the length scales associated with the coherent vortical structures and a 'quasi-laminarization' of the flow downstream of the reaction zone.

The figure also shows that the flame is wrinkled due to the approaching turbulence. The degree of wrinkling of the flame surface increases from the core flow near the centreline towards the inner boundary layer as a consequence of the local increase in the turbulence level. The degree of wrinkling is better observed in figure 6 presenting only the lower half of the computational domain and a smaller number of vortex cores for clarity (light blue isosurfaces). The flame surface is, also in this case, denoted by the reaction progress variable at $C = 0.7$ and coloured by the local temperature. Note that in these figures the reactant side of the flame surface faces the walls in the region between the channel centreline and the viscous layer at $y^+ = 30$. In contrast, for $y^+ < 15$ there is an inversion of the flame surface inclination due to the low flow velocity that allows the flame to creep upstream, locally, even in the presence of strong temperature gradients towards the 'cold' solid surface. Details of the flame surface orientation close to the wall can be seen in the magnified enclosure of figure 5.
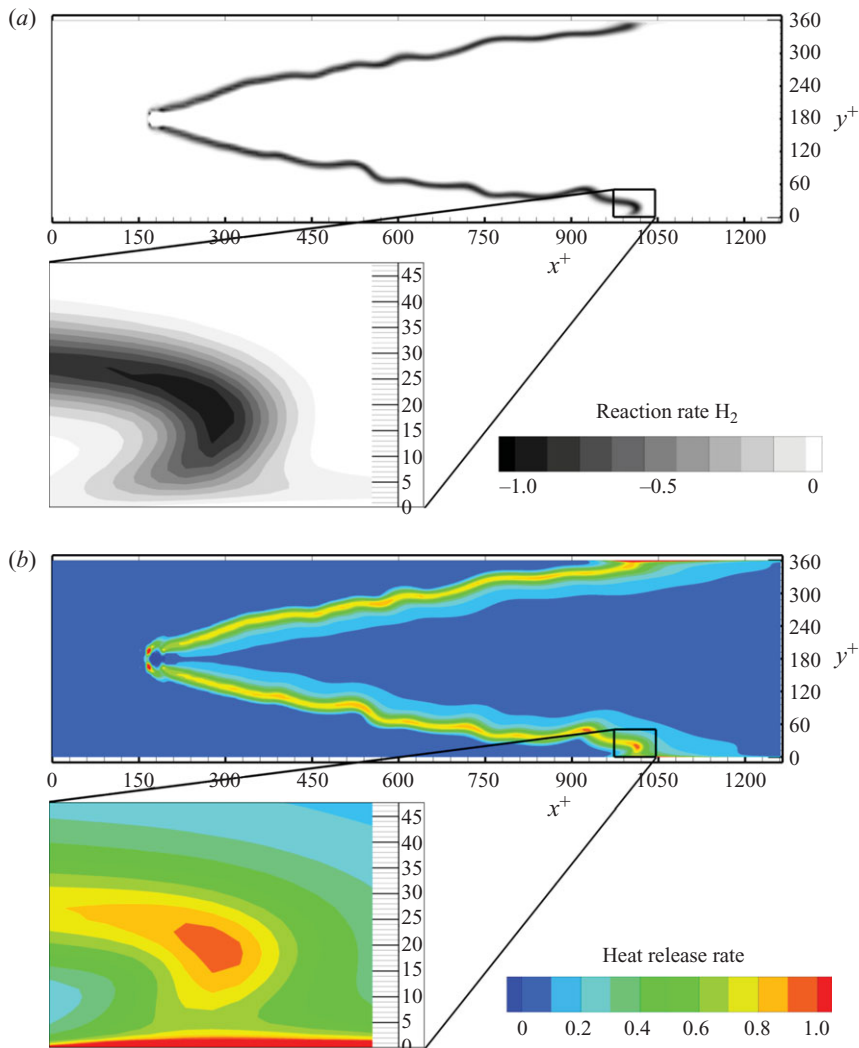
FIGURE 7. Instantaneous snapshots of a streamwise-transverse plane in the computational domain as in figure 5. The flow direction is from left to right. Instantaneous fields of normalized hydrogen reaction rate (*a*) and heat release rate (*b*) normalized by the corresponding values from a freely propagating laminar flame. The insets show a zoom of the near-wall region.

Figure 7 shows contours of instantaneous H_2 reaction rate (figure 7*a*) and of heat release rate (figure 7*b*) on a streamwise-transverse plane normalized by the corresponding quantities from a freely propagating laminar flame. The insets show a zoom of the region near the wall. Interestingly, the reaction rate of hydrogen vanishes close to the wall, indicating 'local extinction' of the flame while the heat release rate decreases only slightly in the vicinity of the wall and then attains a peak again at the wall. This observation indicates the presence of two different reaction modes, one describing the flame in the core flow and the other describing the behaviour at the wall where the radical recombination reactions are dominant and responsible for the large heat release rate. These observations are consistent with the laminar
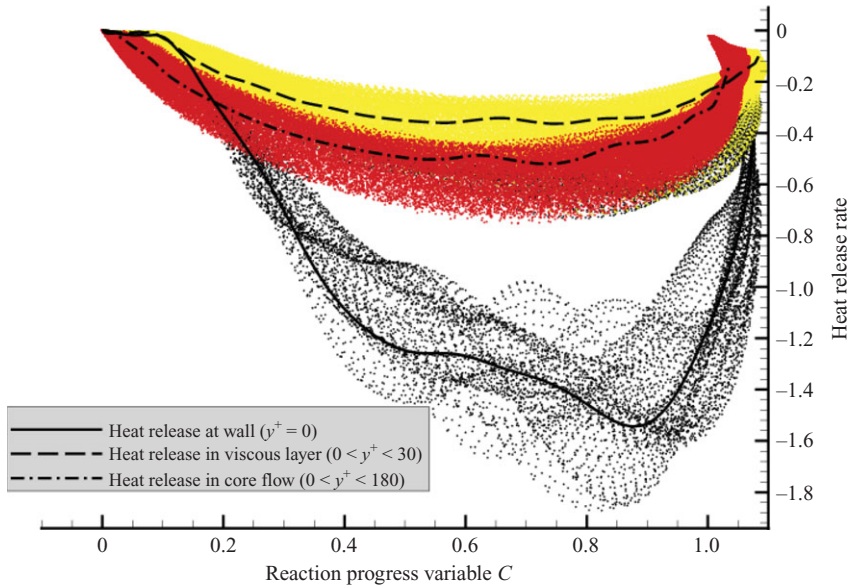
FIGURE 8. Scatter plot of the normalized heat release rate against the reaction progress variable C for the core flow region (dot-dashed line and red points), in the viscous layer (dashed line and yellow points) and at the wall (solid line and black points). Lines represent curve fit of the ensemble of data points. The heat release rate of the freely propagating flame is used for normalization.

results presented in §4.1 and with a scatter plot of the instantaneous heat release rate versus progress variable that is shown in figure 8. This figure clearly shows a bi-modal reaction pattern. An analysis of the reaction-wise contributions to this (not shown) confirms the importance of radical recombination reactions 8, 9 and 11 to the overall heat release rate at the wall, as per the laminar case.

The flow configuration chosen in the present work allows spatial averaging in the homogeneous spanwise direction, z^+, in addition to time averaging, and therefore good statistics can be obtained after a relatively 'short' simulation time of 230 wall time units or $\sim 1.0\,e^{-03}$ (s). Figure 9 shows the averaged fields of temperature (figure 9a) and reaction progress variable (figure 9b). The vertical solid lines denote the streamwise locations of the y–z planes selected for statistical analysis of relevant quantities presented in the following paragraphs. The black dashed lines denote the average position of the reaction zone based on the averaged reaction progress variable isosurface, $\overline{C} = 0.7$. The characteristic v-shape of the anchored flame is evident. The turbulent flame speed S_t is estimated from the mean centreline velocity U_c, and from the average shape of the v-flame (determined by the angle between the flame surface and the channel centreline). S_t is found to be approximately 1.5 times larger than the laminar flame speed of the corresponding freely propagating flame.

It is interesting to note that the average thickness of the flame zone, bounded between $\overline{C} = 0.05$ and $\overline{C} = 0.95$ and coloured in green in the bottom figure, increases as the boundary layer is approached, becoming notably thicker at $x^+ = 930$ ($y^+ = 36$) than at $x^+ = 310$ ($y^+ = 144$). The flame thickness increases for two reasons. First, the increased unsteadiness and wrinkling of the 'instantaneous' flame brush results in an increase of the 'averaged' flame zone thickness. Second, the turbulent length and time scales that characterize the motion of the eddies in the approaching turbulence
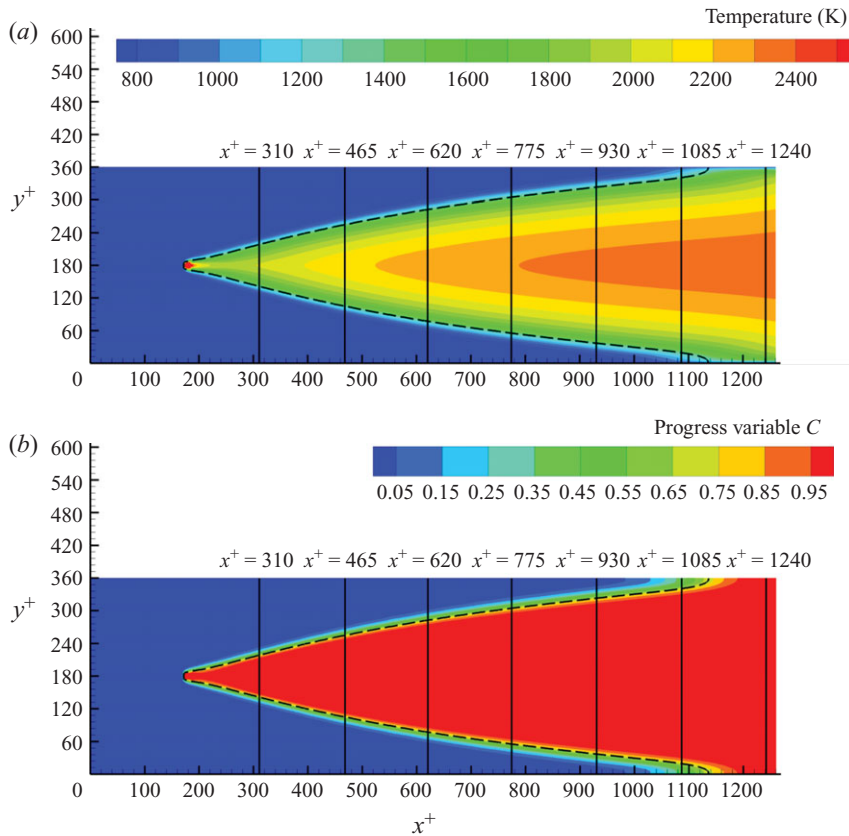
FIGURE 9. Mean temperature (*a*) and reaction progress variable $\overline{C}$ fields (*b*), where the averaging is performed over time and in the spanwise direction (z^+). In both plots the dashed black lines demarcate the surface defined by a representative value of the reaction progress variable at $\overline{C} = 0.7$. The vertical black lines indicate the streamwise locations for statistical analysis presented in the following figures.

decrease as the distance from the wall is reduced. Conversely, the chemical time scales become larger due to heat loss. This leads to a decrease in the local Damköhler number and to entrainment of small eddies in the flame reactive zone suggesting that the flame may undergo a regime change from the 'thin flamelet' combustion regime near the channel centreline to a 'thickened wrinkled' regime closer to the wall (Borghi 1988).

To quantify the broadening of the instantaneous flame thickness, the gradient $|\nabla C|$ of the reaction progress variable C is used as a measure of the flame thickness, where values above the reference laminar flame thickness indicate flame thinning and below represent broadening Sankaran *et al.* (2006). As an illustrative example $|\nabla C|$ is plotted against C for two premixed laminar flames with different equivalence ratios and thus different flame thicknesses in figure 10(*a*): the fuel lean ($\phi = 0.3$), thicker laminar flame is characterized by a maximum value of $|\nabla C|$ that is approximately half as large as that of the fuel rich ($\phi = 1.5$), thinner flame. The broadening of the flame zone for decreasing wall distance is confirmed by the probability density function (p.d.f.) of $|\nabla C|$ shown in figure 10(*b*), where the gradient is calculated at $C = 0.7$. The p.d.f.s are constructed at selected streamwise locations, that is, for several different
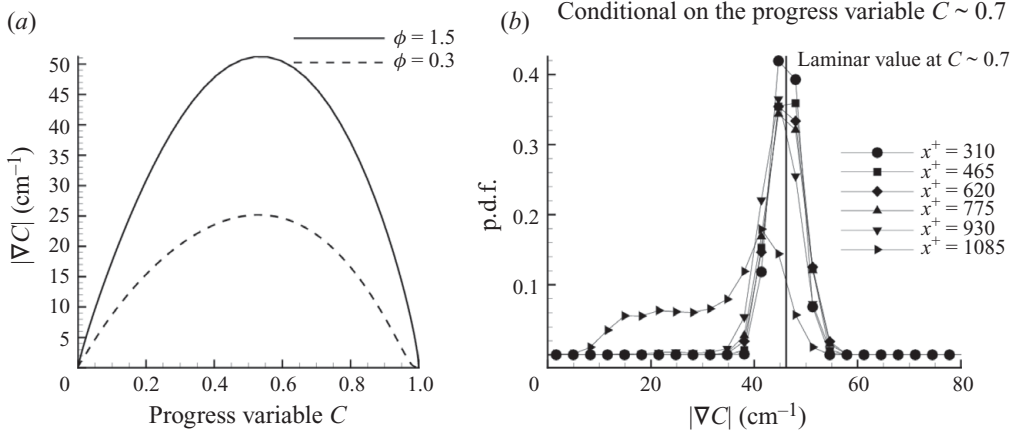
FIGURE 10. The reaction progress variable gradient $|\nabla C|$ as a function of C for two laminar flames with different equivalence ratios (a). Probability density function of the reaction progress variable gradient $|\nabla C|$ at $C = 0.7$ for selected streamwise positions (flame–wall distances), the laminar flame value of $|\nabla C|$ at $C = 0.7$ is indicated with a vertical line (b).
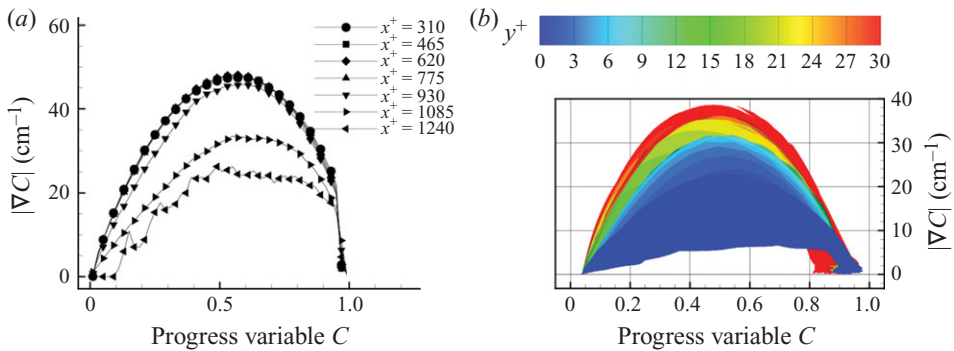

FIGURE 11. Mean values of the reaction progress variable gradient $|\nabla C|$ as a function of C for selected streamwise flame positions (a) and in the viscous layer (b) The coloured bands indicate the non-dimensional wall distance y^+.

distances between the flame and the wall. Whereas the mean and most probable values of $|\nabla C|$ (and consequently of the flame thickness) are nearly unchanged for the interval $310 < x^+ < 775$ ($60 < y^+ < 144$), they show a small but noticeable decrease (i.e. the flame thickens) for $x^+ \sim 930$ ($y^+ \sim 36$) and a considerable reduction for $x^+ \sim 1085$ ($y^+ \sim 20$) where the p.d.f. also becomes skewed to lower values of $|\nabla C|$ indicating the occurrence of large flame thicknesses.

Figure 11(a) presents the progress variable conditionally-averaged values of $|\nabla C|$ for selected streamwise flame positions and as a function of the non-dimensional wall distance in the viscous layer for $0 < y^+ < 30$ (figure 11b), the latter figure shows the non-dimensional wall distance doubly conditional on progress variable and $|\nabla C|$. Both figures confirm the conjecture that close to the wall, significant broadening of the preheat layer occurs. This is an interesting finding for modelling of turbulent combustion since models may be required to transition from flamelet to more distributed reaction modes within a single combustor (Peters 1997).
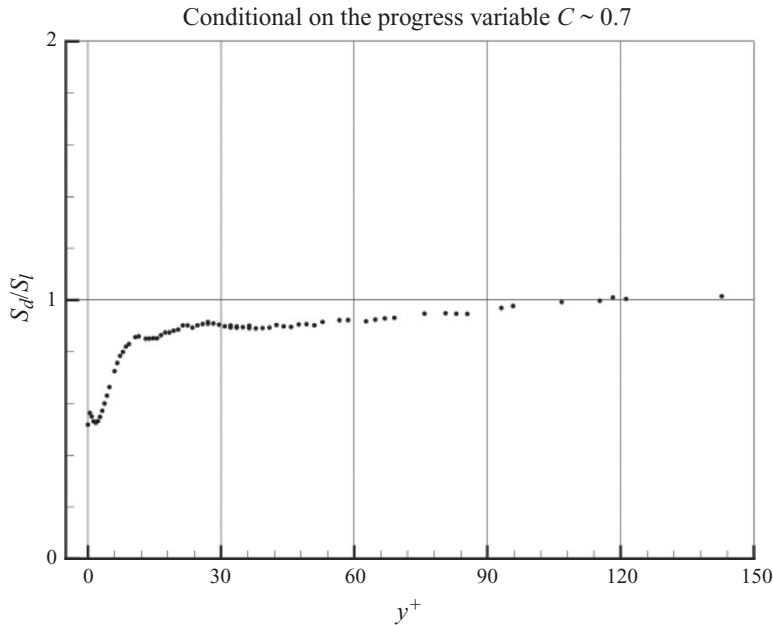
Conditional on the progress variable $C \sim 0.7$

FIGURE 12. Averaged displacement speed S_d, normalized by the laminar flame speed, of the reaction progress variable as a function of the distance from the wall y^+.

To examine the local propagation characteristics, the local displacement speed S_d of a C-isosurface is examined. The displacement speed is defined, as in previous studies (Gibson 1968; Pope 1988; Poinsot, Echekki & Mungal 1992; Echekki & Chen 1999; Hawkes & Chen 2004; Chakraborty, Klein & Cant 2006),

$$S_d = \frac{1}{|\boldsymbol{\nabla} C|} \frac{\mathrm{D}C}{\mathrm{D}t}.$$

In figure 12 the averaged displacement speed S_d (normalized by S_l) is plotted for $C = 0.7$ against the non-dimensional wall distance y^+. Near the centreline, the flame speed is nearly constant and close to the freely propagating laminar value. However at approximately $y^+ \sim 15$ it decreases by a factor of 2. This finding is significant for models of turbulent premixed combustion that assume a constant flame speed close to the laminar value. The decrease in flame speed is a consequence of the vanishing H_2 reaction rate at the wall as discussed in figure 7(a). However, it is interesting to note that despite the reaction rate becoming negligible at the wall, the flame speed does not vanish – this is because there is a non-negligible contribution from diffusion tangential to the flame surface contributing to the flame speed, causing a net non-zero propagation rate. The modelling of this effect is a topic that is beyond the scope of the present paper but deserves further investigation.

Finally, we examine the strain rate that is known to affect both the local flame speed and the generation of flame surface area (see Veynante & Vervisch 2002). Figure 13 shows the p.d.f. of tangential strain rate acting on the scalar isosurface $C = 0.7$ at selected streamwise locations along the channel. Symmetric, relatively narrow p.d.f.s are observed in the core flow region while considerably broader p.d.f.s are clearly visible in the more turbulent region closer to the wall, indicating an increase in the magnitude of strain (both positive and negative) acting on the flame. This may be a consequence of the orientation of the flame brush. For $y^+ < 30$, the flame brush is

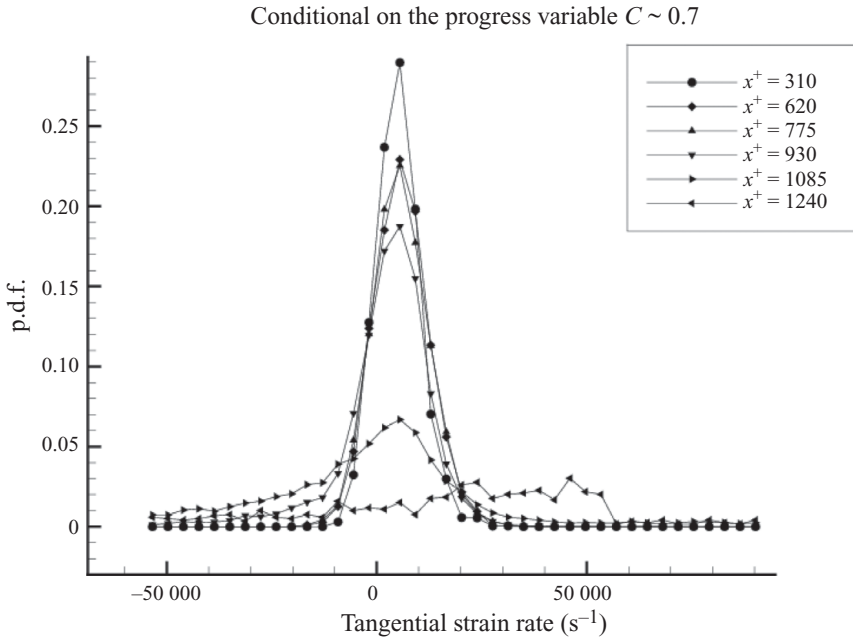Conditional on the progress variable $C \sim 0.7$

FIGURE 13. Probability density function of the tangential strain rate acting on the scalar isosurface $C = 0.7$ for selected streamwise positions.

frequently parallel to the wall and to the flow direction resulting in increased mean strain rate on the flame, such that positive strain becomes predominant for $x^+ > 1000$. Once more we note that the inclusion of these effects in models for turbulent premixed combustion such as the flame-surface density approach may be required if accurate predictions of near-wall behaviour is desired (see Veynante & Vervisch 2002; Cant, Pope & Bray 1990; Hawkes 2000).

4.2.2. *Convective wall heat transfer*

In the recent development of small-sized gas turbines, notoriously characterized by large heat transfer and low combustion efficiency, heat transfer by conduction is higher than in larger engines because the temperature gradients are higher as the characteristic length is decreased (see Fernandez-Pello 2002). Also, as the characteristic length scales of the devices are reduced, the surface-to-volume ratio increases which results in more prominent heat transfer effects and flame quenching. Accordingly, the 'mean' values of the heat flux into the wall must be accurately estimated for optimal design of cooling devices while, on the other hand, their 'maximum' values and fluctuation length scales and frequencies have a direct influence on the lifetime of the combustor (fatigue failure).

First, the 'mean' wall-heat flux is investigated. Figure 14 shows the averaged heat flux along the channel length: the maximum averaged wall heat flux ($\sim 1.4\,(\mathrm{MW\,m^{-2}})$) is 1.14 times the laminar value at quenching and it is attained at 1043 wall units downstream of the inflow boundary at the position where the FWI occurs most frequently. Downstream of this position the cooling of the hot burnt products of reaction causes a decay of the wall heat flux ($\sim 1.0\,(\mathrm{MW\,m^{-2}})$) to 0.8 times the laminar HOQ maximum value.
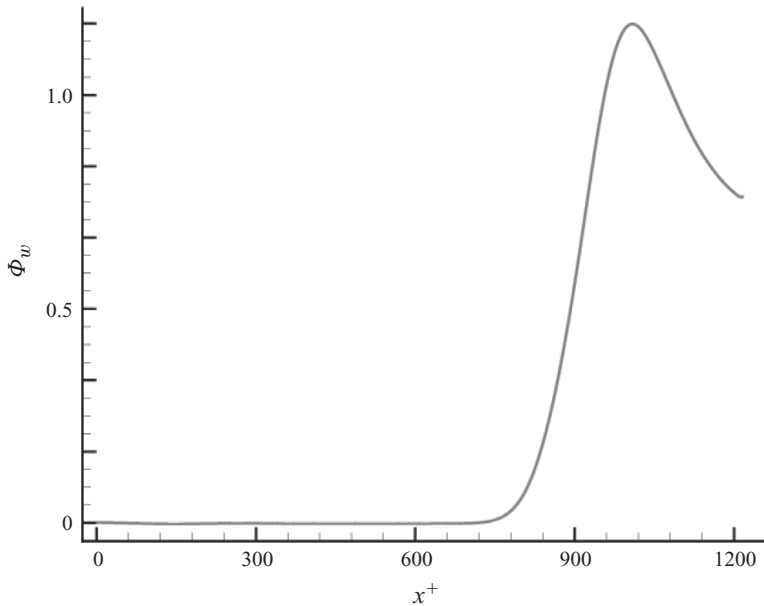
FIGURE 14. Normalized averaged wall heat flux along the channel length. The wall heat flux is normalized by the laminar HOQ value from the one-dimensional case.
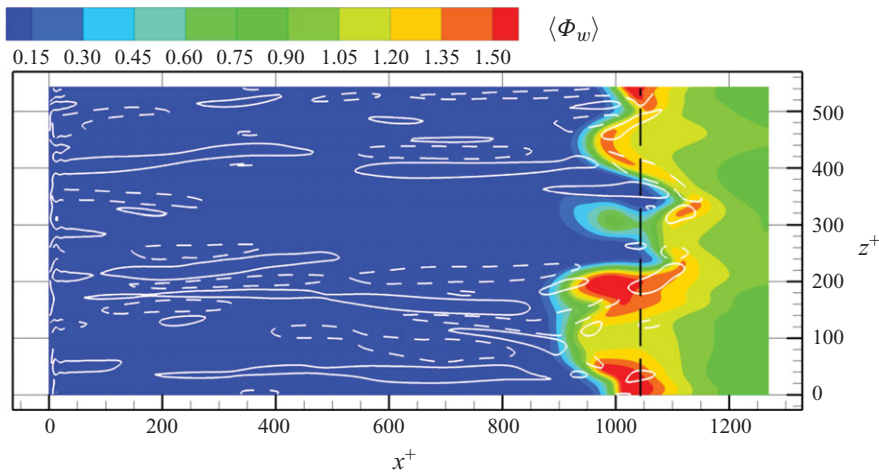

FIGURE 15. Instantaneous snapshot of the normalized wall heat flux Φ_w (blue-to-red isocontours) onto the lower wall at $y^+ = 0$ and of the quasi-streamwise streaky vorticity structures (white isolines) demarcated by wall-normal vorticity at $y^+ = 5$. The wall heat flux in the three-dimensional case is normalized by the laminar HOQ value from the one-dimensional case.

To provide a more local, instantaneous picture, figure 15 shows an instantaneous snapshot of the wall heat flux at $y^+ = 0$ (blue-to-red isocontours) and of the wall-normal vorticity in the viscous sublayer at $y^+ = 5$ (white lines). Wall-normal vorticity at $y^+ = 5$ is a good marker of the streaky quasi-streamwise structures of the boundary layer. The dashed and solid white lines indicate different directions of rotation ($10\,000$ and $-10\,000\,(1\,\mathrm{s}^{-1})$). The vorticity lines upstream of the FWI are in good agreement

with boundary-layer turbulence theory showing several structures elongated in the flow direction and characterized by streamwise lengths of the order of 300 wall units, with spanwise dimension and spacing of approximately 30 and 100 wall units, consistent with Kim *et al.* (1987) and Jiménez (1998), respectively. Also, the observed average turnover time of the streamwise vorticity structures compares well with the estimate of 16 wall time units given by Orlandi & Jiménez (1994), while the observed average velocity at which these structures are convected downstream is equal to approximately half of the centreline average velocity U_c. Kim & Hussain (1994) suggest a typical value for this convective velocity equal to 55 % of U_c. Considering the non-dimensional centreline velocity for the present case $u_c^+ \sim 19$, this average convective velocity is $0.55 u_c^+ \sim 11$ and provides an average value of $300/11 \sim 27$ wall time units for the typical 'passage time' of the near-wall streamwise vorticity structures past a fixed streamwise location.

The maxima in the wall heat flux are linked both to convective motions and to reactions occurring at the wall. Reactionwise analysis of the heat release rate in the vicinity of the wall (not shown) indicates that the local peaks in the instantaneous wall heat flux in figure 15 are strongly correlated with the peaks in the heat release rate caused by the most active radical recombination reaction (reaction 8 in the mechanism of table 1). Similar results are found for the other radical recombination reactions, confirming the importance of radical chemistry in the heat transfer to the wall during FWI. This suggests that consideration of radical recombination reactions at the wall is required to obtain a quantitatively accurate description of the FWI process.

To investigate in more detail the unsteady convective aspects of the wall heat flux, figure 16 illustrates a temporal sequence (*a* to *j*) of instantaneous snapshots of the wall heat flux similar to that in figure 15, spaced 1.8 wall time units τ_w apart. The solid and dashed white lines indicate vortical structures of opposite sign. It is interesting to observe how the pairs of counter-rotating vortical structures enter the domain from the inlet boundary on the left, are convected downstream and finally interact with the flame brush in the vicinity of the $x^+ \sim 1000$. Also, the isocontours of wall heat flux show a characteristic pattern of a number of transient high-intensity wall heat flux locations ('hot spots') that appear to be induced by the pairs of counter-rotating vortical structures. These 'hot spots' are, similar to the vorticity streaks, characterized by a spanwise spacing of the order of 100 wall units. This length scale is denoted, l_e, for the remainder of this discussion. Direct observation of all other instantaneous fields suggests that these maximum wall heat flux locations are born, grow, migrate and decay, on a time scale t_e, while maintaining, on average, the same spanwise spacing, l_e. Also, these wall locations are subject to a wall heat flux of the same order of magnitude of the flux observed in the laminar case reported in §4.1. The magnitude in the turbulent case is larger or smaller than the laminar case depending on the local turbulent flow pattern and on the angle of impingement of the flame onto the wall. As suggested by Poinsot *et al.* (1993) and by Alshaalan & Rutland (1998), the underlying physical process behind the observed spatial and temporal pattern of the wall heat flux is related to the structure of boundary-layer turbulence. More precisely, it is related to the presence of the near-wall quasi-streamwise vorticity structures that alternately push the flame towards the wall, causing quenching and large heat release rate on one side of the streamwise vortex, and push it away on the other, thereby inducing large spanwise gradients of the heat transfer into the wall.

The aforementioned average spacing and time scale that characterize the FWI process and the observed maximum wall heat flux pattern are also investigated by spectral analysis of the DNS data: the instantaneous value of the wall heat flux is
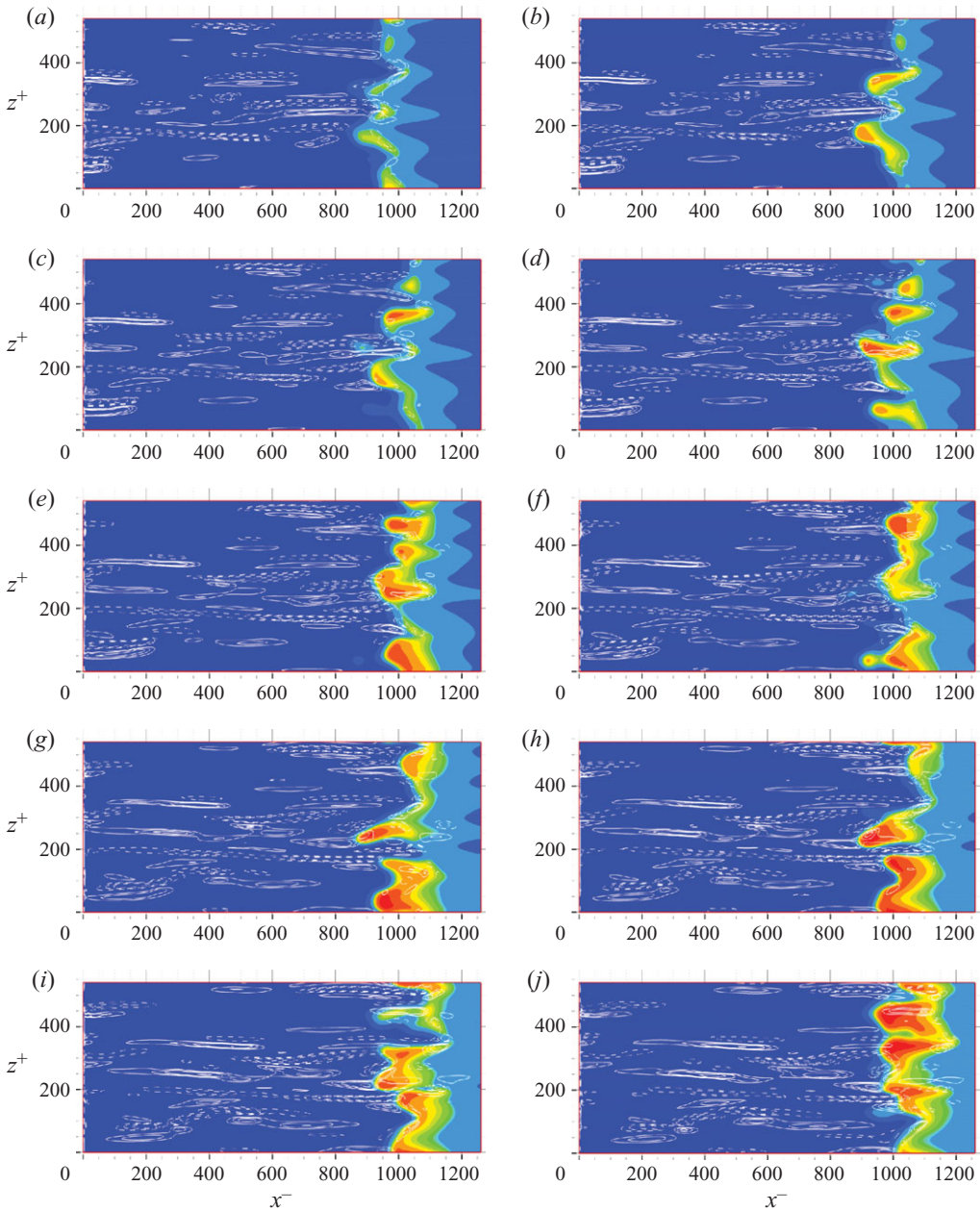
FIGURE 16. A sequence $(a–j)$ of instantaneous snapshots showing the wall heat flux Φ_w (blue-to-red colour scale) onto the lower wall at $y^+ = 0$ and the quasi-streamwise streaky vorticity structures (white lines) marked by wall-normal vorticity at $y^+ = 5$.

collected for each of the 88 samples on both the upper and the lower wall in a line along the spanwise direction at $x^+ = 1043$. The sampling location corresponds to the location of the maximum wall average as shown in figure 14. The collected data are shown versus time and spanwise distance in figure 17. To analyse these data quantitatively, they are then Fourier transformed to wavenumber space resulting in spatial and a temporal spectra.
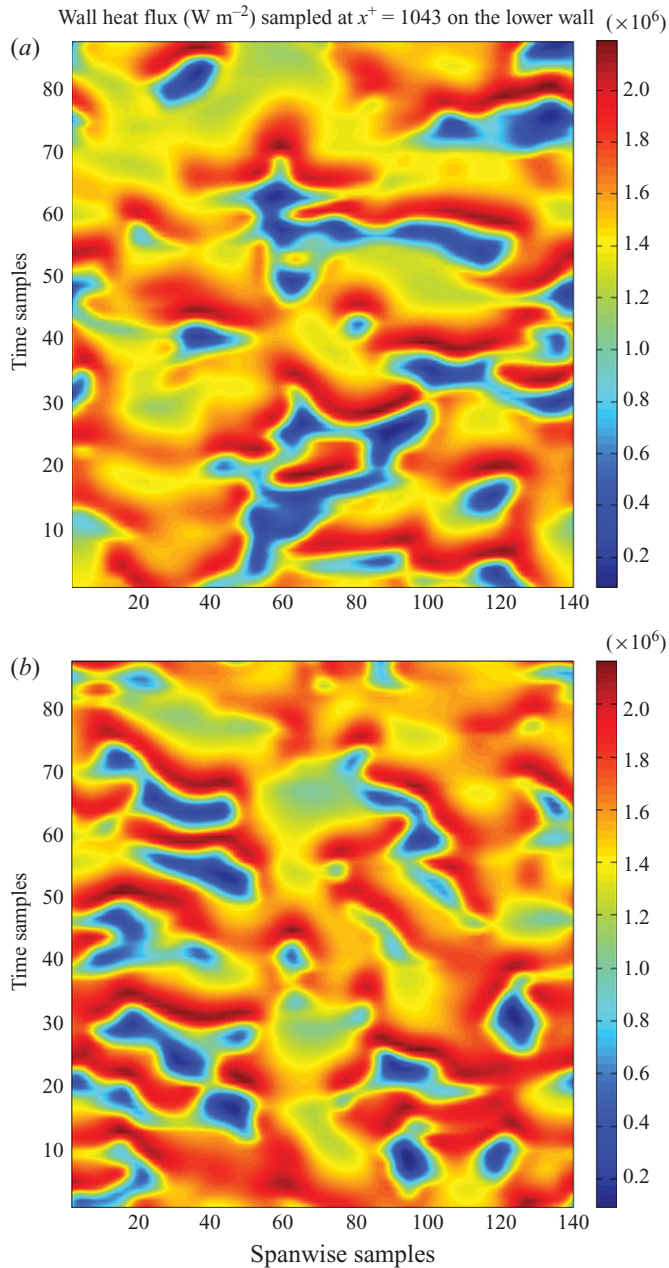
Wall heat flux (W m^{-2}) sampled at $x^{+} = 1043$ on the lower wall $(\times 10^6)$

$(\times 10^6)$

Spanwise samples

FIGURE 17. Values of the instantaneous wall heat flux sampled at $x^{+} = 1043$ for 88 time steps on both the lower and upper wall.

The resulting spectra are plotted in figure 18. The spatial spectrum peaks at a frequency corresponding to a spanwise spacing of 100 wall units, and the l_e length scale is demarcated by a black rectangle. The order of magnitude of this length scale is consistent with prior studies of wall heat transfer in a non-reacting flow (Abe, Kawamura & Matsuo 2004). However, the curved shape and slope of the spectrum appear to be different compared to what is commonly observed in analogous wall
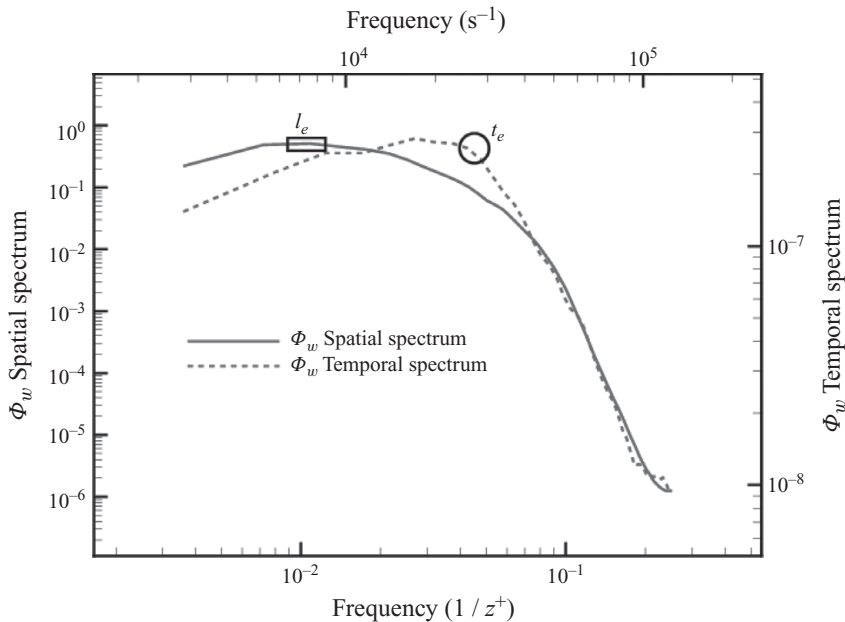
Frequency (s^{-1})

FIGURE 18. Spatial and temporal spectrum of the fluctuating wall heat flux sampled at $x^+ = 1043$ and normalized by their integral in Fourier space.

heat flux spanwise spectra computed for passive scalar transport. Figure 4 in the paper by Abe *et al.* (2004) shows, for $Re_\tau = 180$, an approximately flat profile to $1/z^+ \sim 10^{-1}$, and then a steeper slope towards the small scales. This difference may be attributable to the fact that in the present case there is a propagating flame, and not a passively transported scalar. The propagation introduces its own length and time scales into these spectra.

The temporal spectrum shows that large fluctuations of the wall heat flux take place in a range of time scales between 10 and 26 wall time units (the flat plateau between 9–27 kHz). These time-scales may be compared with those of the near-wall streamwise vorticity structures. The average half-turnover time is 8 wall time units (complete turnover estimated as 16 wall time units) and the 'passage time' past the flame–wall impingement region is 27 wall time units. Therefore, we conclude that the observed relevant temporal scaling in the fluctuations of the wall heat flux is highly correlated with the near-wall streamwise vorticity structures.

Finally, the p.d.f. of the instantaneous wall heat flux sampled at $x^+ = 1043$ is shown in figure 19. The p.d.f. exhibits a long negative skewness. This indicates that the flame frequently impinges onto the wall at or upstream of the sampling location. Therefore, the occurrences of 'low' heat transfer into the wall (in the range 0.2–1.0 (MW m^{-2})) are relatively rare.

The above observations can be summarized as follows: in the near-wall region of the turbulent flow the spatial displacement of the flame is influenced by the presence of elongated quasi-streamwise vortical structures that, in some regions, push the flame sheet away from the wall causing a local decrease in the convective wall heat flux, while in other adjacent regions push the flame towards the wall, increasing heat loss, exothermic radical recombination reactions, heat release rate and wall heat flux, ultimately leading to the quenching of the flame.
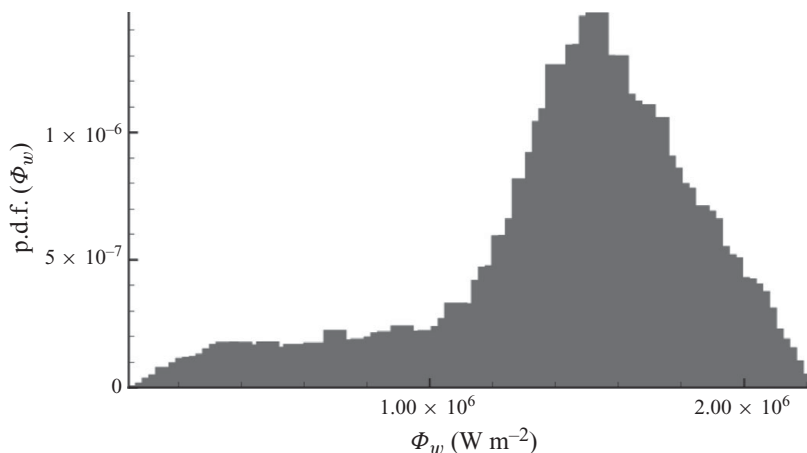
FIGURE 19. Probability density function of the instantaneous wall heat flux sampled at $x^+ = 1043$.

5. Conclusions and further work

One-dimensional DNS of laminar HOQ and three-dimensional DNS of turbulent FWI in a plane channel flow have been reported for a premixed hydrogen–air flame.

The results for the laminar flames confirmed the conclusions of previous studies by Dabireau *et al.* (2003). The quenching distance and maximum wall heat flux have similar non-dimensional values and radical recombination plays a major role in increased heat release rate at the wall.

In the turbulent case, the flow of the fresh reactants approaching the flame front is characterized by $Re_\tau = 180$. The turbulent flame investigation focused on the following two issues: the interaction between the flame front and the turbulent boundary layer, and the effect of the boundary-layer structures on the wall heat flux.

The discussion in §4.2.1 indicates strong effects of the flame front on the approaching turbulence whose characteristic length scales undergo a relatively abrupt change across the reaction zone. At the same time, the turbulence affects the flame structure and thickness that changes as a function of the distance from the walls. Near the channel centreline, the flame thickness is approximately the laminar flame thickness while close to the wall the results show a considerable thickening of the flame. This indicates 'a combustion regime change' from a 'thin flamelet' regime near the channel centreline to a 'thickened wrinkled' regime, close to the wall. Furthermore, examination of the local flame propagation speed indicates a sharp two-fold decrease towards the wall, again indicating a possible regime change. Interestingly, the flame speed does not drop to zero despite a vanishing reaction rate, indicating an increased importance of the diffusional contributions to flame speed at the wall. Finally, we find that the tangential flame strain varies significantly from the centreline to the wall, with much higher values occurring near the wall. All of these findings have considerable implications for turbulent combustion models if wall-bounded flames are to be captured. They show that one must account for (i) a regime change towards the wall to a thickened flame regime, (ii) a reduced but non-zero local flame speed at the wall and (iii) effects of the wall on flame stretch. Further examination of these questions would provide fruitful avenues for future studies. For example, the importance of these effects relative to those already included in turbulent combustion

models could be assessed by a larger parametric study spanning different modes of FWI.

As for the heat flux induced by the flame brush into the solid wall, an average spanwise spacing of 100 wall units in the spatial pattern of the maximum wall heat flux locations correlates well with the presence of characteristic coherent streamwise vorticity structures as predicted by boundary-layer theory. Also, the observed temporal pattern associated with the heat flux fluctuation correlates well with the characteristic time scales of the boundary-layer vorticity structures. Large wall heat fluxes occur on time and length scales that are comparable to the elongated vorticity structures 'rotation-passage time', and to the near-wall streamwise vorticity structures average spanwise spacing, equal to 100 wall units. Accordingly, we postulate that turbulent FWI is governed by the presence of near-wall turbulent vorticity structures that push the flame towards the wall on one side and away from it on the other, thereby inducing large spanwise gradients of the heat transfer into the wall. These variations are 'amplified by radical recombination' that cannot be captured by simple-chemistry DNS. An approach that could be explored in the future is whether the amplifying effect could be captured using a simple canonical configuration such as a transient HOQ in a laminar wall-jet flow. We also note that at higher Reynolds number, large 'superstructures' have been observed in turbulent wall-bounded flows Hutchins & Marusic (2007a, b) that could lead to locally enhanced wall heat-transfer by similar mechanisms to those discussed in this study. If these superstructures have a similar effects on FWI in general and on the wall heat transfer in particular, the time and length scales involved would be significantly larger, something that, in turn, could induce large thermal stresses in the solid material.

The results presented here are significant for the application of large-eddy simulation to FWI. Whereas in open flows, much is gained by the direct resolution of the large scales of flame wrinkling (Hawkes & Cant 2001) at high Reynolds number in wall-bounded flows, this may not be feasible. The relevant wrinkling scales of FWI are the near-wall turbulence structures, and at high Reynolds number the resolution of these structures on the computational grid becomes unaffordable (Pope 2000). As a result, most practitioners resort to using Reynolds-averaged Navier–Stokes type wall models. The situation will be analogous for FWI, and unless the wall structures are directly resolved, considerably more will be required of the subgrid models compared with open flows. A promising direction for further work in this area would be an examination of the effects of the wall on premixed combustion models used in Reynolds-averaged Navier–Stokes or large-eddy simulation.

Further work is recommended to perform DNS at higher Reynolds number and including surface chemistry effects. In particular, the former may be significant for practical devices operating at sufficiently high bulk flow speed, in the boundary-layer large velocity variations may occur over short distances comparable with the flame thickness and the local flow velocity may exceed the laminar flame speed within a short distance from the wall. As for the latter, a reactive surface, under some specific conditions, would act as a catalyst adsorbing and recombining radicals and possibly changing the radical balance in the chemical kinetics of the gas phase. The effect these phenomena may have on the FWI needs to be addressed in targeted studies because extrapolation of the results presented here from low to high Reynolds number and from inert to reactive surfaces appear as a challenging endeavour.

REFERENCES

ABE, H., KAWAMURA, H. & MATSUO, Y. 2004 Surface heat-flux fluctuations in a turbulent channel flow up to $re_\tau = 1020$ with $pr = 0.025$ and 0.71. *J. Heat Fluid Flow* **25**, 404–419.

ALSHAALAN, T. M. & RUTLAND, C. J. 1998 Turbulence, scalar transport, and reaction rates in flame-wall interaction. In *Proceedings 27th International Symposium on Combustion* (ed. Anthony R. Burgess & Frederick L. Dryer), pp. 793–799. The Combustion Institute.

ALSHAALAN, T. M. & RUTLAND, C. J. 2002 Wall heat flux in turbulent premixed reacting flow. *Combust. Sci. Technol.* **174**, 135–165.

BELLENOUE, M., KAGEYAMA, T., LABUDA, S. A. & SOTTON, J. 2004 Direct measurements of laminar flame quenching distance in a closed vessel. *Exp. Therm. Fluid Sci.* **27**, 323–331.

BORGHI, R. 1988 Turbulent combustion modelling. *Prog. Energy Combust. Sci.* **14**, 245–292.

BRUNEAUX, G., AKSELVOLL, K., POINSOT, T. & FERZIGER, J. H. 1996 Flame-wall interaction simulation in a turbulent channel flow. *Combust. Flame* **107**, 27–44.

CANT, R. S., POPE, S. B. & BRAY, K. N. C. 1990 Modelling the flame surface to volume ratio in turbulent premixed combustion. In *Proceedings 23rd International Symposium on Combustion* (ed. William J. McLean & Pamela K. Barr), pp. 809–815. The Combustion Institute.

CHAKRABORTY, N., KLEIN, M. & CANT, R. S. 2006 Stretch rate effects on displacement speed in turbulent premixed flame kernels in the thin reaction zones regime. In *Proceedings 31st International Symposium on Combustion* (ed. Robert S. Barlow, Volker Sick, Peter Glarborg & Richard A. Yetter), pp. 1385–1392. The Combustion Institute.

CHEN, J. H., CHOUDHARY, A., DE SUPINSKI, B., DEVRIES, M., HAWKES, E. R., KLASKY, S., LIAO, W. K., MA, K. L., MELLOR-CRUMMEY, J., PODHORSZKI, N., SANKARAN, R., SHENDE, S. & YOO, C. S. 2009 Terascale direct numerical simulations of turbulent combustion using s3d. *Comput. Sci. Discovery* **2**, 015001.

DABIREAU, F., CUENOT, B., VERMOREL, O. & POINSOT, T. 2003 Interaction of flames of $H_2 + O_2$ with inert walls. *Combust. Flame* **135**, 123–133.

DOMINGO, P., VERVISCH, L., PAYET, S. & HAUGUEL, R. 2005 DNS of a premixed turbulent v-flame and LES of a ducted flame using a fsd-pdf subgrid scale closure with fpi-tabulated chemistry. *Combust. Flame* **143**, 566–586.

ECHEKKI, T. & CHEN, J. H. 1999 Analysis of the contribution of curvature to premixed flame propagation. *Combust. Flame* **118**, 308–311.

ECHEKKI, T. & CHEN, J. H. 2003 Direct numerical simulation of autoignition in non-homogeneous hydrogen–air mixtures. *Combust. Flame* **134**, 169–191.

ENOMOTO, M. 2002 Sidewall quenching of laminar premixed flames propagating along the single wall surface. In *Proceedings 29th International Symposium on Combustion* (ed. Jacqueline H. Chen & Meredith D. Colket), pp. 781–787. The Combustion Institute.

EZEKOYE, O., GREIF, R. & SAWYER, R. F. 1992 Increased surface temperature effects on wall heat transfer during unsteady flame quenching. In *Proceedings 24th International Symposium on Combustion* (ed. Chung K. Law), pp. 1465–1472. The Combustion Institute.

FERNANDEZ-PELLO, A. C. 2002 Micropower generation using combustion: Issues and approaches. In *Proceedings 29th International Symposium on Combustion* (ed. Jacqueline H. Chen & Meredith D. Colket), pp. 883–899. The Combustion Institute.

FRITZ, J., KRÖNER, M. & SATTELMAYER, T. 2004 Flashback in a swirl burner with cylindrical premixing zone. *ASME J. Engng. Gas Turbines Power* **126**, 276–283.

GIBSON, C. H. 1968 Fine structure of scalar fields mixed by turbulence. Part I. Zero-gradient points and minimal gradient surfaces. *Phys. Fluids* **11**, 2305–2315.

GRUBER, A. 2006 Direct numerical simulation of turbulent combustion near solid surfaces. PhD thesis, Energy Processes Department, Norwegian University of Science and Technology, Trondheim, Norway.

HAWKES, E. R. 2000 Large eddy simulation of premixed turbulent combustion. PhD thesis, Engineering Department, University of Cambridge, Cambridge, UK.

HAWKES, E. R. & CANT, R. S. 2001 Physical and numerical realizability requirements for flame surface density approaches to large eddy and Reynolds averaged simulation of premixed turbulent combustion. *Combust. Theory Modelling* **5**, 699–720.

HAWKES, E. R. & CHEN, J. H. 2004 Evaluation of models for flame stretch due to curvature in the thin reaction zones regime. In *Proceedings 30th International Symposium on Combustion* (ed. Jacqueline H. Chen, Meredith D. Colket, Robert S. Barlow & Richard A. Yetter), pp. 647–656. The Combustion Institute.

HAWKES, E. R. & CHEN, J. H. 2005 Comparison of direct numerical simulation of lean premixed methane-air flames with strained laminar flame calculations. *Combust. Flame* **144**, 112–125.

HAWKES, E. R., SANKARAN, R., SUTHERLAND, J. C. & CHEN, J. H. 2006 Scalar mixing in direct numerical simulations of temporally evolving plane jet flames with skeletal CO/H_2 kinetics. In *Proceedings 31st International Symposium on Combustion* (ed. Robert S. Barlow, Volker Sick, Peter Glarborg & Richard A. Yetter), pp. 1633–1640. The Combustion Institute.

HOCKS, W., PETERS, N. & ADOMEIT, G. 1981 Flame quenching in front of a cold wall under two-step kinetics. *Combust. Flame* **41**, 157–170.

HUNT, J. C. R., WRAY, A. A. & MOIN, P. 1988 Eddies, stream and convergence zones in turbulent flows. *Tech. Rep.* CTR-S88. Center for Turbulence Research, Stanford University, Stanford, CA.

HUTCHINS, N. & MARUSIC, I. 2007a Evidence of very long meandering structures in the logarithmic region of turbulent boundary layers. *J. Fluid Mech.* **579**, 1–28.

HUTCHINS, N. & MARUSIC, I. 2007b Large-scale influences in near-wall turbulence. *Phil. Trans. R. Soc.* A **365**, 647–664.

JIMÉNEZ, J. 1998 The largest scales of turbulent wall flows. In *Annual Research Briefs of the Center for Turbulence Research* (ed. Parviz Moin), pp. 137–154. Stanford University, Stanford, CA.

JIMÉNEZ, J. & MOIN, P. 1991 The minimal flow unit in near wall turbulence. *J. Fluid Mech.* **225**, 213–240.

KEE, R. J., DIXON-LEWIS, G., WARNATZ, J., COLTRIN, M. E., MILLER, J. A. & MOFFAT, H. K. 1999 A fortran chemical kinetics package for the analysis of gas-phase chemical kinetics. *Tech. Rep.* Release 3.5. Reaction Design Inc., San Diego, CA.

KENNEDY, C. A. & CARPENTER, M. H. 1994 Several new numerical methods for compressible shear-layer simulations. *Appl. Numer. Math.* **14** (0), 397–433.

KENNEDY, C. A., CARPENTER, M. H. & LEWIS, R. M. 2000 Low-storage, explicit Runge–Kutta schemes for the compressible Navier–Stokes equations. *Appl. Numer. Math.* **35** (0), 177–219.

KIM, J. 1983 On the structure of wall-bounded turbulent flows. *Phys. Fluids* **26**, 2088–2097.

KIM, J. & HUSSAIN, F. 1994 Propagation velocity of perturbations in turbulent channel flow. *Phys. Fluids* **5**, 695–706.

KIM, J., MOIN, P. & MOSER, R. 1987 Turbulence statistics in fully developed channel flow at low Reynolds number. *J. Fluid Mech.* **177**, 133–166.

LI, J., ZHAO, Z., KAZAROV, A. & DRYER, F. L. 2004 An updated comprehensive kinetic model of hydrogen combustion. *Intl J. Chem. Kinetics* **36**, 566–575.

LIGNELL, D. O., CHEN, J. H., SMITH, P. J., LU, T. & LAW, C. K. 2007 The effect of flame structure on soot formation and transport in turbulent nonpremixed flames using direct numerical simulation. *Combust. Flame* **151**, 2–28.

MOSER, R., KIM, J. & MANSOUR, N. 1999 Direct numerical simulation of turbulent channel flow up to $Re_\tau = 590$. *Phys. Fluids* **11** (4), 943–945.

NG, T. T., CHENG, R. K., ROBBEN, F. & TALBOT, L. 1982 Combustion-turbulence interaction in the turbulent boundary layer over a hot surface. In *Proceedings 19th International Symposium on Combustion* (ed. Jack B. Howard), pp. 359–366. The Combustion Institute.

ORLANDI, P. & JIMÉNEZ, J. 1994 On the generation of turbulent wall friction. *Phys. Fluids* **6**, 634–641.

PETERS, N. 1997 The turbulent burning velocity for large-scale and small-scale turbulence. *J. Fluid Mech.* **384**, 107–132.

PITSCH, H. 2006 Large eddy simulation of turbulent combustion. *Annu. Rev. Fluid Mech.* **38**, 453–482.

POINSOT, T., ECHEKKI, T. & MUNGAL, M. G. 1992 A study of the laminar flame tip and implications for premixed turbulent combustion. *Combust. Sci. Technol.* **81**, 45–73.

POINSOT, T., HAWORTH, D. C. & BRUNEAUX, G. 1993 Direct simulation and modelling of flame-wall interaction for premixed turbulent combustion. *Combust. Flame* **95**, 118–132.

POINSOT, T. & LELE, S. K. 1992 Boundary conditions for direct simulations of compressible viscous flow. *J. Comput. Phys.* **101**, 104–129.

POPE, S. B. 1988 The evolution of surfaces in turbulence. *Intl J. Engng Sci.* **26**, 445–469.

POPE, S. B. 2000 *Turbulent Flows*, 2nd edition. Cambridge: Cambridge University Press.

POPP, P. & BAUM, M. 1997 Analysis of wall heat fluxes, reaction mechanisms, and unburnt hydrocarbons during the head-on quenching of a laminar methane flame. *Combust. Flame* **108**, 327–348.

POPP, P., SMOOKE, M. & BAUM, M. 1996 Heterogeneous/homogeneous reaction and transport coupling during flame-wall interaction. In *Proceedings 26th International Symposium on Combustion*, pp. 2693–2700. The Combustion Institute.

ROBINSON, S. K. 1991 Kinematics of turbulent boundary layer structure. *Tech. Rep.* TM-103859. Moffet Field, NASA.

RUNSTADLER, P. W., KLINE, S. J. & REYNOLDS, W. C. 1963 An investigation of the flow structure of the turbulent boundary layer. *Tech. Rep.* 8. Department of Mechanical Engineering, Stanford University, Stanford University, Stanford, CA.

SANKARAN, R., HAWKES, E. R., CHEN, J. H., LU, T. & LAW, C. K. 2006 Structure of a spatially developing turbulent lean methane–air bunsen flame. In *Proceedings 31st International Symposium on Combustion* (ed. Robert S. Barlow, Volker Sick, Peter Glarborg & Richard A. Yetter), pp. 1291–1298. The Combustion Institute.

SANKARAN, R., IM, H. G., HAWKES, E. R. & CHEN, J. H. 2004 The effects of non-uniform temperature distribution on the ignition of a lean homogeneous hydrogen–air mixture. In *Proceedings 30th International Symposium on Combustion* (ed. Jacqueline H. Chen, Meredith D. Colket, Robert S. Barlow & Richard A. Yetter), pp. 875–882. The Combustion Institute.

SUTHERLAND, J. C. & KENNEDY, C. A. 2003 Improved boundary conditions for viscous, reactive, compressible flows. *J. Comput. Phys.* **191**, 502–524.

VEYNANTE, D. & VERVISCH, L. 2002 Turbulent combustion modelling. *Prog. Energy Combust. Sci.* **28**, 193–266.

WESTBROOK, C. K., ADAMCZYK, A. A. & LAVOIE, G. A. 1981 A numerical study of laminar flame wall quenching. *Combust. Flame* **40**, 81–99.